Methionine-stevensite derived bionanocomposite: A green and efficient adsorbent for the removal of antibiotics

Moaad Gharous [a,b], Julia Martín [c,*], Carmen Mejías [c], Loubna Bounab [a], Mohamed Choukairi [b], Juan Luis Santos [c], Irene Aparicio [c], Esteban Alonso [c]

[a] Research Group of Advanced Materials, Structures and Civil Engineering, National School of Applied Sciences of Tetouan, Abdelmalek Essaadi University, BP 2121, Tetouan 93002, Morocco
[b] Laboratory of Materials Engineering and Sustainable Energy (LMESE), Faculty of Science, Abdelmalek Essaadi University, BP 2121, Tetouan 93002, Morocco
[c] Departamento de Química Analítica, Escuela Politécnica Superior, Universidad de Sevilla, Seville E-41011, Spain

ABSTRACT

The persistent appearance of antibiotic residues in the aquatic ecosystem is considered an issue of great concern. This study examined the adsorptive efficiency of a novel bionanocomposite (L-methionine/stevensite, MET/ST) for promising decontamination of nine antibiotics. Results revealed that MET/ST allows an excellent antibiotic removal efficiency, from 87% for trimethoprim (TMP) to almost 100% for the eight remaining antibiotics, at neutral pH, an adsorbent dose of 2 g/L, and 1.5 mg/L of the antibiotics mixture. Equilibrium was achieved in less than 1 min, except for TMP (30 min), and the kinetics was consistent with the pseudo-second order model (R^2 > 0.927). The isotherm data were fitted with the Langmuir and Freundlich models (R^2 > 0.960) (q_{max} from 21.48 to 28168 mg/g for TMP and chlortetracycline, respectively). The high surface area (170.49 m^2/g) and pore volume (0.16 cm^3/g) of MET/ST, together with electrostatic and hydrogen bonding interactions, played a dominant role in antibiotic adsorption. TMP was the only antibiotic affected by temperature (from 61% to 85% at 5 and 45ºC) and salinity (from 87% to 37% at 0 and 4% *w/v* of NaCl). The MET/ST was used consecutively for at least four adsorption–desorption cycles after being regenerated with a capacity > 97% in the last cycle for 7 out of 9 antibiotics. In addition to its adsorption capacity, reusability and low-cost features, the material demonstrated an excellent efficiency (up to 69% for TMP and 100% for other antibiotics) in wastewater and surface water samples denoting a great application for water purification.

1. Introduction

Antibiotics are one of the most frequently prescribed therapeutic groups because of their broad spectrum of applications to treat bacterial infections. The excreta after administration contributes to its release into sewer system, and, if not properly removed in wastewater treatment plants (WWTPs), ultimately in the environment (Mejías et al., 2021). In effect, more than 50% of antibiotics used are estimated to end up in the environment through discharges from hospitals and wastewater effluents (Dutta and Mala, 2020). This

concern has motivated the European Union to develop regulations on ecosystem protection. Up to eight antibiotics have been included in the Watching List (WL) of emerging water pollutants under the Water Framework Directive (European Commission, 2020; 2018; 2022). The macrolides azithromycin (AZM), clarithromycin (CTM), and erythromycin (ERY) were first incorporated in the WL of 2015. Then, in 2018, ciprofloxacin (CIP) and amoxicillin were added into a second WL. In 2020, the WL maintained the monitoring of CIP and amoxicillin and incorporated sulfamethoxazole and trimethoprim (TMP). The most recent version of the WL, in 2022, still maintains the monitoring of sulfamethoxazole and TMP, and incorporates the antibiotic ofloxacin (OFL). Antibiotics have been found in wastewater at high concentrations relative to other pharmaceuticals analysed (Delgado et al., 2023). For example, concentration levels of up to 8.3 µg/L for TMP have been found in influent wastewater from Peru (Nieto-Juarez et al., 2021). In effluent wastewater from Singapore, concentrations reached up to 1.5 µg/L for tetracycline (TC) and 2.0 µg/L for chlortetracycline (CTC) (Tran et al., 2016).

Several techniques have been proposed to remove antibiotics from wastewater (Chaturvedi et al., 2021) including photo-degradation (Cao et al., 2019), oxidation (Anjali and Shanthakumar, 2019), ozonation, adsorption (Attallah et al., 2016; Imanipoor et al., 2021a,b), nanofiltration (Zhao et al., 2018) or biological treatments (Oberoi et al., 2019).

Among them, adsorption is recognized as one of the most cherished techniques owing to its design simplicity, economic feasibility and, higher efficacy (Ben Amor et al., 2023; Kolya and Kang, 2023; Khan and Khan, 2021; Haciosmanoglu et al., 2022; 2023). In last years, nanohybrid materials prepared by the incorporation of biopolymers into layered silicates have received significant attention covering the main individual flaws of clays (regeneration issue) and polymers (low mechanical strength and/or poor water wettability) (Al-Hazmi et al., 2014; Martín et al., 2023). These materials combine the structural and textural properties of clay with the functionality of the guest biopolymer, which result in materials that have a significant increase in Young's modulus, ion conductivity, higher efficacy, regeneration assets, surface area, barrier resistance, and tensile strength in addition to being cost-effective (Pereira et al., 2021; Martín et al., 2023). Furthermore, the control of biopolymer-clay interactions will help in the development of smart nanomaterials for environmental applications (Orta et al., 2020; Khan and Khan, 2021). Some combinations such as chitosan–alginate–bentonite, alginate-bentonite, chitosan-bentonite, methionine-montmorillonite have been proposed to remove some antibiotics such as AZM (Imanipoor et al., 2021a), ampicillin, doripenem, amoxicillin (Yeo et al., 2023), or TC (Filho et al., 2023).

Within the ample range of adsorbents employed for an environmental cause, bionanocomposite based on amino acid-clay are emerging as an attractive materials platform for water purification, owing to their high sorption capacity, affinity, environmental viability, tailorable physiochemical characteristics, and better reusability (Ahmad and Ezaj, 2023; Imanipoor et al., 2021a; 2021b). The presence of –OH, –COOH and $-NH_2$ in the amino acid structure along with the adsorptive potential of clays validate them as a hot spot sorbent. This study examines the adsorptive efficiency of a novel bionanocomposite (L-methionine/stevensite, MET/ST) for promising decontamination of a group of nine widely prescribed antibiotics. ST is a trioctahedral smectite with layer charge derived from vacant octahedral positions and characterized by its numerous advantages such as large specific surface area, hydrophilicity, chemical reactivity, and lack of toxicity. Some works have highlighted the mineralogical characterisation of ST from the Atlas Mountains of Morocco (called locally "Rhassoul") as adsorbent in the water treatment field (Naboulsi et al., 2022; Fernández et al., 2018; Ajbary et al., 2013). MET is a promising nontoxic biomolecule in the field of pollutant trapping due to its carboxylic, thiol, and amino ligand side chain (Ahmad and Mirza, 2015; Faghihian and Nejati-Yazdinejad, 2009). To the best of our knowledge, modification of ST with natural amino acids has not been reported up to now. The antibiotic adsorption was investigated altering the environmental conditions (presence of dissolved organic matter, pH, and ionic strength). Furthermore, MET/ST reusability and potential application with real wastewater and surface water samples were examined.

2. Methods

2.1. Reagents and materials

High purity standards ($\geq$ 95%) of ofloxacin, CIP, roxithromycin (RXM), CTC and TC were supplied by Sigma-Aldrich (Steinheim, Germany). TMP was purchased from Dr Ehrenstorfer GmbH (Augsburg, Germany). AZM was provided by the European Pharmacopoeia Reference Standard (Strasbourg, France). ERY and CTM were supplied by Tokyo Chemicals Industry (Eschborn, Germany). Their physico-chemical properties can be seen in Table S1.

Ammonium formate, MET amino acid and humic acid were supplied by Sigma-Aldrich (Madrid, Spain). Hydrochloric acid, formic acid, sodium hydroxide, and sodium chloride were provided by Panreac (Barcelona, Spain). All of them were analytical grade. LC-MS-grade methanol and water were purchased from Biosolve BV (Valkenswaard, The Netherlands).

The clay used in this work is Rhassoul, a moroccan lava clay located in Jebel Rhassoul, in the mountains of the Atlas of Morocco. This clay is rich in ST (69.048% SiO_2, 18.878% MgO, 4.656% Al_2O_3, 0.397% TiO_2, 1.360% CaO, 1.291% K_2O, 0.216% Na_2O, 0.573% P_2O_5, 0.014% Cr_2O_3, 0.191% SrO, 0.098% SO_3, 3.251% Fe_2O_3, and 0.026% MnO).

2.2. Preparation of amino acid-modified stevensite (MET/ST bionanocomposite)

First, the raw clay was washed with distilled water, dried, milled, and sieved. The clay was then treated as described by Ben Seddik et al. (2019). An amount of 30 g of washed clay were shacked for 30 min in 1 L of bidistilled water. After 30 min, drops of HCl (1 M) were gradually added until the last bubble of CO_2, to the decomposition of carbonates. To facilitate clay modification and to increase the interfacial distance, the clay is homoionized with Na^+ cations. For that the powder resulting from decarbonisation were dispersed in NaCl solution (1 M) by shaking for 12 h and separated by centrifugation. The resulting Na^+-ST was added to a 2 L test tube to isolate

fine particles of less than 2 μm of diameter according to the Stokes law equation.

The clay nanocomposite was organomodified by the intercalation process as described by Imanipoor et al. (2021b). Briefly, 4 g of the resulting clay was added to 100 mL of deionized water and stirred at 80 °C for more than 3 h. A mass of MET representing 1.5 CEC of the used clay was prepared in 50 mL of deionized water and protonated using HCl and stirred at 80°C. Then, both solutions were homogenized and stirred at 60°C for 6 h. MET is an amino acid with a thioether side chain containing a sulfur atom. At acidic medium, the amino group tends to be protonated, gains a proton carrying a positive charge. This positive charge can interact with the negatively charged sites on the clay surface, according to the equation: $ST/Na + MET^+ \rightarrow ST/MET + Na^+$

The resulting solution was then filtered 3 times (4200 rpm, 10 min) and oven dried at 50°C for 24 h. Finally, the resulting MET/ST bionanocomposite was ground in a mortar.

2.3. Characterization analysis

The characterization of the MET/ST derived bionanocomposite was carried out before and after the adsorption experiments. Scanning electron microscopy and energy dispersive X-ray spectroscopy (SEM-EDS) analyses were performed by a FEI-TENEO scanning electron microscope (FEI, USA). X-ray diffraction (XRD) analysis was carried out using a Bruker D8 Advance A25 diffractometer (Bruker, Germany). Fourier transform-infrared spectroscopy (FT-IR) analysis was conducted with a Cary 630 FT-IR (Agilent, USA). N_2 adsorption isotherms were carried out with a gas sorption analyzer ASAP 2420 (accelerated surface and porosimetry system) (Micromeritics Instrument, UK). The zeta potential and particle size analyses were measured using a Zetasizer Nanosystem (Malver Instruments, USA).

2.4. Batch adsorption assays

Batch adsorption studies were conducting using a mixture of antibiotic solution at 1500 ng/mL, pH 7.5, and 25 °C, except those in which concentration, pH and temperature were tested. An adsorbent dose of 2 g/L was kept constant by shaking 20 mg of MET/ST with 10 mL of aqueous solutions. The influence of the environmental conditions (presence of dissolved organic matter, pH, and ionic strength) was investigated. The summary of the conditions applied in each batch of experiments are found in Table S2.

After each experiment, the water and the adsorbent phases were separated by centrifugation at 4000 rpm for 5 min. The remaining concentration of antibiotics in the water solution was measured using a liquid chromatography tandem mass spectrometry instrument (LC-MS/MS) (Agilent, Santa Clara, USA). The chromatographic and determination conditions were previously described in Mejías et al. (2022) and summarized in the Supplementary material (Table S3).

The removal and adsorption capacity of antibiotics was calculated using the Eqs. (1) and (2), respectively.

$$R = (C_0 - C_e)/C_0 \cdot 100 \tag{1}$$

$$q_e = V \cdot (C_0 - C_e)/m \tag{2}$$

Where C_0 and C_e (mg/L) are the antibiotic concentrations in the water solution at the beginning and the end of the adsorption test. V is
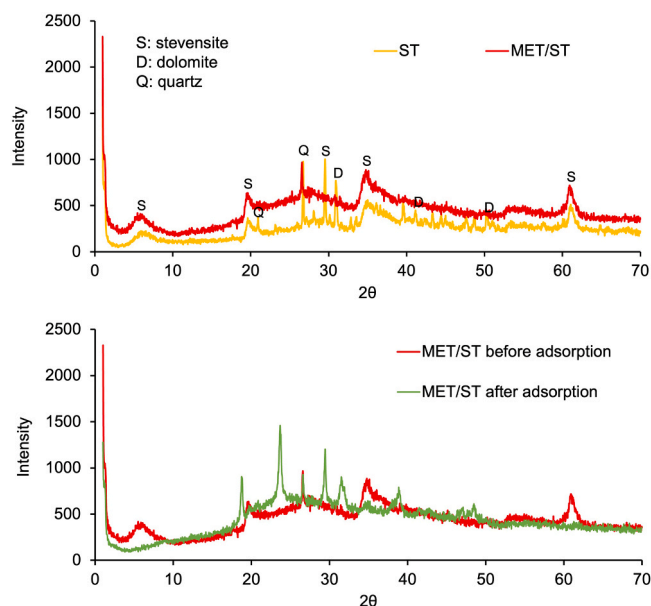

Fig. 1. DRX pattern of ST and derived MET/ST bionanocomposite (upper). DRX pattern of MET/ST before and after antibiotic adsorption (down).

the water solution volume (0.01 L) and m is the MET/ST amount (0.02 g).

3. Results and discussion

3.1. Characterization of raw materials and derived MET/ST bionanocomposite

ST is a natural clay known for its high crystallinity and its high specific surface area. The N_2 adsorption results revealed a BET surface area of 147 m^2/g and a pore volume of 0.08 cm^3/g. Compared to ST, the organomodified MET/ST composite presented a higher specific surface area (170 m^2/g) and pore volume (0.16 cm^3/g) (Table S4). Similarly, the researchers reported that this effect may be related to the deposition amino acids on the clay surface (Chu et al., 2020; Kuroki et al., 2014). A type II isotherm was obtained for the raw ST and the derived bionanocomposite (Figure S1) which suggests the presence of mesopores and typically associated with materials with well-defined pore structures. The flatter region in the medium represents the formation of a monolayer. At very low pressures, the micropores fill in with nitrogen gas and the monolayer formation begins. Multilayer formation occurs at medium pressure while capillary condensation appears at higher pressures. Type II isotherms show a gradual convex upward curve shape at low concentrations, followed by a sharp concave upward data trend (Brião et al., 2022). The pore diameter is in the order of 5.76 nm and 7.01 nm for ST and MET/ST respectively. SEM was used to observe changes in surface morphology of ST and the resulting MET/ST bionanocomposite. Figure S2 shows the clay in the form of agglomerates consisting of irregular layers of varying micrometer sizes, which is typical of smectite clay (Moussout et al., 2020; Ahrouch et al., 2019; Bentahar et al., 2019), the figure confirms the porous and irregular surface of the MET/ST bionanocomposite. The EDS results support the MET incorporation. The percentage of S, the characteristic element of MET, in the bionanocomposite was strongly increased after the synthesis (from 0% to 5%).

XRD spectra was used to examine the crystalline structure of the adsorbent. Fig. 1 (upper part) shows XRD spectra of ST and the MET/ST bionanocomposite. The XRD pattern showed peaks at 1.32°, 6.08°, 19.65°, 29.53°, 35°, and 48.7°, corresponding to ST (Azaryouh et al., 2023; Allaoui et al., 2020; El Mahbouby et al., 2023). The peak at 60.94° corresponds to the trioctahedral smectite (El Mahbouby et al., 2023). The other peaks are attributed to the associated minerals such as quartz, dolomite, and calcite. After modification, a large number of XRD peaks are eliminated, which is due to the removal of impurities and carbonates during the clay purification procedure by use of hydrochloric acid according to the equation Metal carbonate + 2 HCl → Metal chloride + CO_2 + H_2O, which means that the clay has been purified. The change in particle size after incorporation of the amino acid into the clay interface can also eliminate or displace peaks. Thus, the change in the basal spacing of the ST diffraction peak from 6.08° (1.453 nm) to a low value of 2θ (5.62°, 1.57 nm) confirms the insertion of the protonated amino acid by the ion exchange reaction on the clay with the cationic
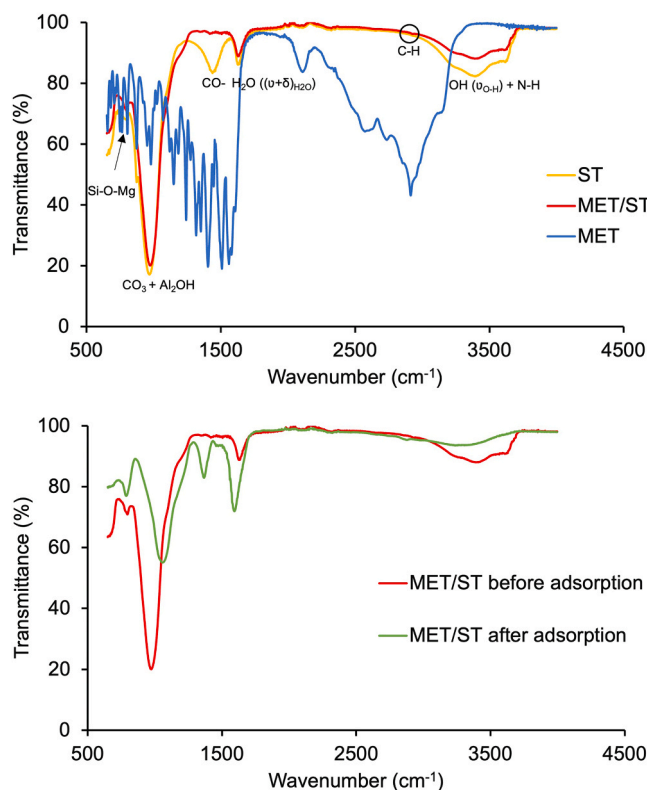

Fig. 2. FTIR spectra of ST, MET and MET/ST bionanocomposite (upper). FTIR spectra of MET/ST before and after antibiotic adsorption (down).
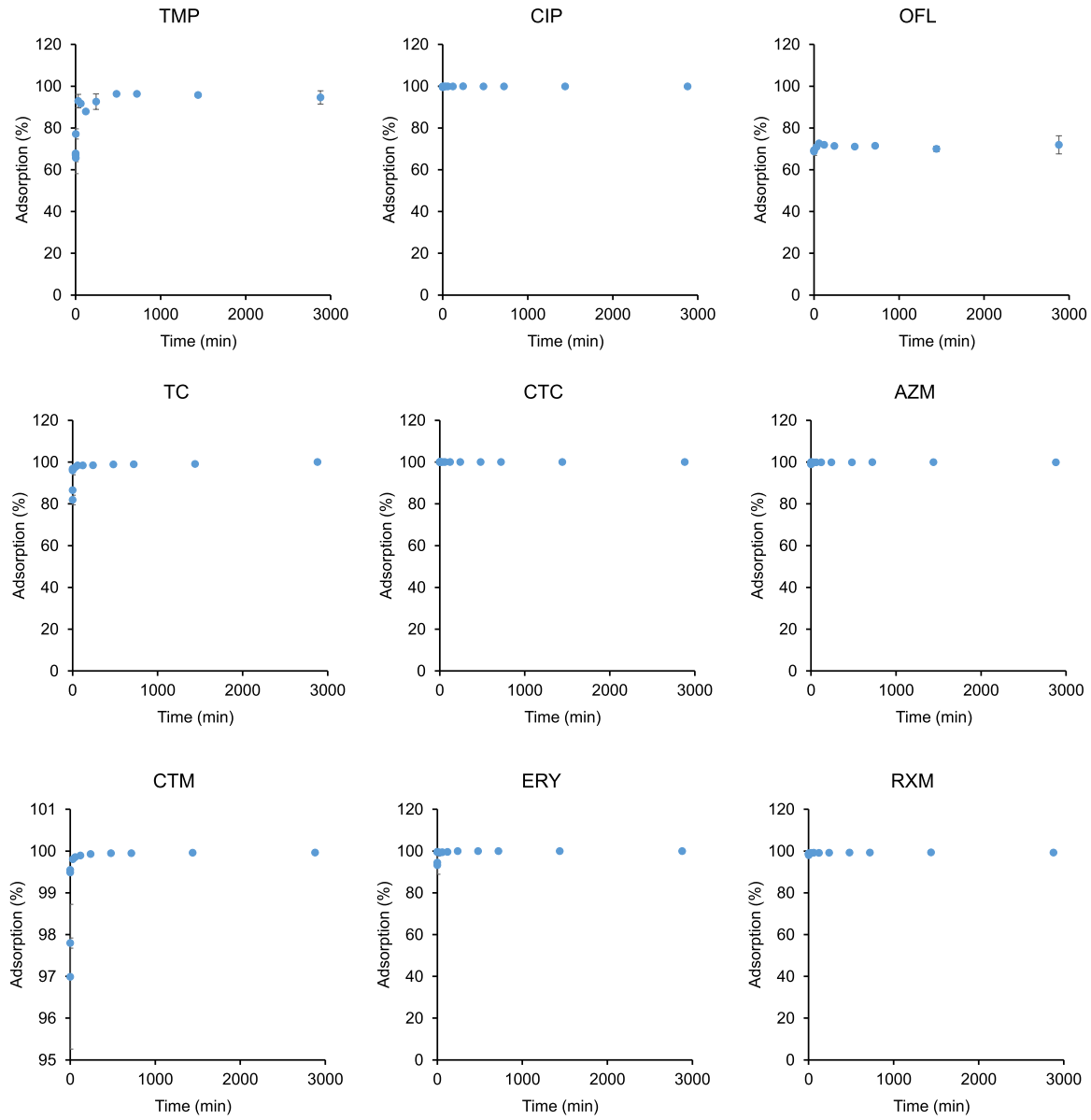
Fig. 3. Adsorption kinetic of solutions of antibiotics onto MET/ST bionanocomposite.

complexes (Ziyat et al., 2020; Brandão-Lima et al., 2022; Kianfar et al., 2014).

The functional groups of MET, ST, and MET/ST bionanocomposite were examined by FTIR spectroscopy (Fig. 2). The FTIR characterization shows five bands for the raw clay (upper part), the first one exists in the high frequency region (3394.89 cm^{-1}) corresponding to the stretching mode of the OH (υ_{O-H}), and two other bands exist in the region of 1630.09 cm^{-1} and 1443.48 cm^{-1}, corresponding to the stretching deformation combination of H$_2$O (($\upsilon+\delta$)$_{H2O}$) and to the CO stretching of carbonates, respectively. In the low-frequency region, there are two bands. An intense band at 966.9 cm^{-1} corresponding to CO$_3$ and Al$_2$OH groups, and another at 784.93 cm^{-1} that can be assigned to the Si-O-Mg group (De Santiago-Buey et al., 2000).

The incorporation of MET into the interlayer space of the clay is not easily detected by FTIR. We noticed the absence of the band at 1443.48 cm^{-1} due to the decarbonisation of the clay, which justifies that the clay was properly treated. The presence of a very fine band at 2924 cm^{-1} (Fig. 2, circle) is due to the C-H stretching of the aliphatic group CH$_2$-S-CH$_3$ because the exchange or substitution of this group with the cations in the raw clay (Imanipoor et al., 2021a; Mallakpour and Dinari, 2011).

The pH$_{ZPC}$ of ST/MET bionanocomposite was 8.2 (Fig. S3).

3.2. Adsorption studies

3.2.1. Kinetic studies

The kinetic study was performed at time (0.083–2880 min), dose (0.02 g), and antibiotic solution (1500 ng/mL). The results are shown in Fig. 3. The adsorption rate of antibiotics on MET/ST was surprisingly very high. At the first 0.5 min, an adsorption efficiency >80% was observed for most compounds and in less than 1 min the equilibrium was achieved for all selected antibiotics, except for TMP (30 min). After equilibrium was reached, no change in capacity was observed with time. Therefore, a contact time of 60 min was selected for the next experiments.

To examine the controlling mechanism of the adsorption process the pseudo first-order and pseudo-second order were correlated to the obtained data (Table 1). The rate constants of the antibiotics adsorption on the bionanocomposite were determined graphically leading to the results summarized in Table 1. According to them, the best fitting of the experimental data was obtained for a pseudo-second order model, as denoted by its higher correlation coefficient (nearly unity (>0.927) for all antibiotics studied). The values of q^e *exp* also agreed well with q^e *cal*. This result is in good agreement with many previous studies employing other clay-based adsorbents to antibiotics (Hacıosmanoglu, et al., 2023; Turan et al., 2022; Imanipoor et al., 2021b).

3.2.2. Isotherm studies

The influence of the concentration of the antibiotics on their adsorption has also been evaluated in a concentration range from 0.5 to 100 mg/L, more than 10000 times higher than those found in wastewater samples (Delgado et al., 2023). The amount of antibiotic adsorbed (q_e), plotted against the equilibrium concentration for each antibiotic, is shown in Fig. 4. The equilibrium isotherms were fitted to Langmuir and Freundlich and linear isotherms (Table 2). Antibiotics were better fitted by the Langmuir model that involved monolayer adsorption with a homogeneous distribution of active sites ($0.963 < R^2 < 0.999$) but were also fitted to the Freundlich model ($0.960 < R^2 < 0.999$). The maximum monolayer sorption capacity, q_{max}, determined with the Langmuir isotherm, was high, from 21.48 mg/g for TMP to > 110 mg/g for the rest of antibiotics, and follows the order: CTC > CTM > RXM > ERY > TC > OFL > AZM > CIP > TMP. The n parameter of the Freunlich model was > 1, which means that adsorption was favourable (Mustapha et al., 2019). Imanipoor et al. (2021a,b) reported that AZM was adsorbed on MET-montmorillonite following a Freundlich isotherm model (q_{max} 298.78 mg/g) while amoxicillin was adsorbed following a Langmuir isotherm model (q_{max} 647.7 mg/g). In a recent work, Filho et al. (2023) observed an adsorption capacity of 178.65 mg/g for TC onto chitosan-alginate-bentonite fitting to a Langmuir isotherm model. Similarly, doripenem, amoxicillin, and ampicillin were successfully removed with chitosan-bentonite (96, 86.1 and 83.3 mg/g, respectively) using a Langmuir isotherm model (Yeo et al., 2023).

Thermodynamic studies were carried out in the temperature range from 5 to 45 °C. The adsorption capacities of MET/ST were

Table 1
Kinetic parameters for adsorption of antibiotics onto MET/ST bionanocomposite.

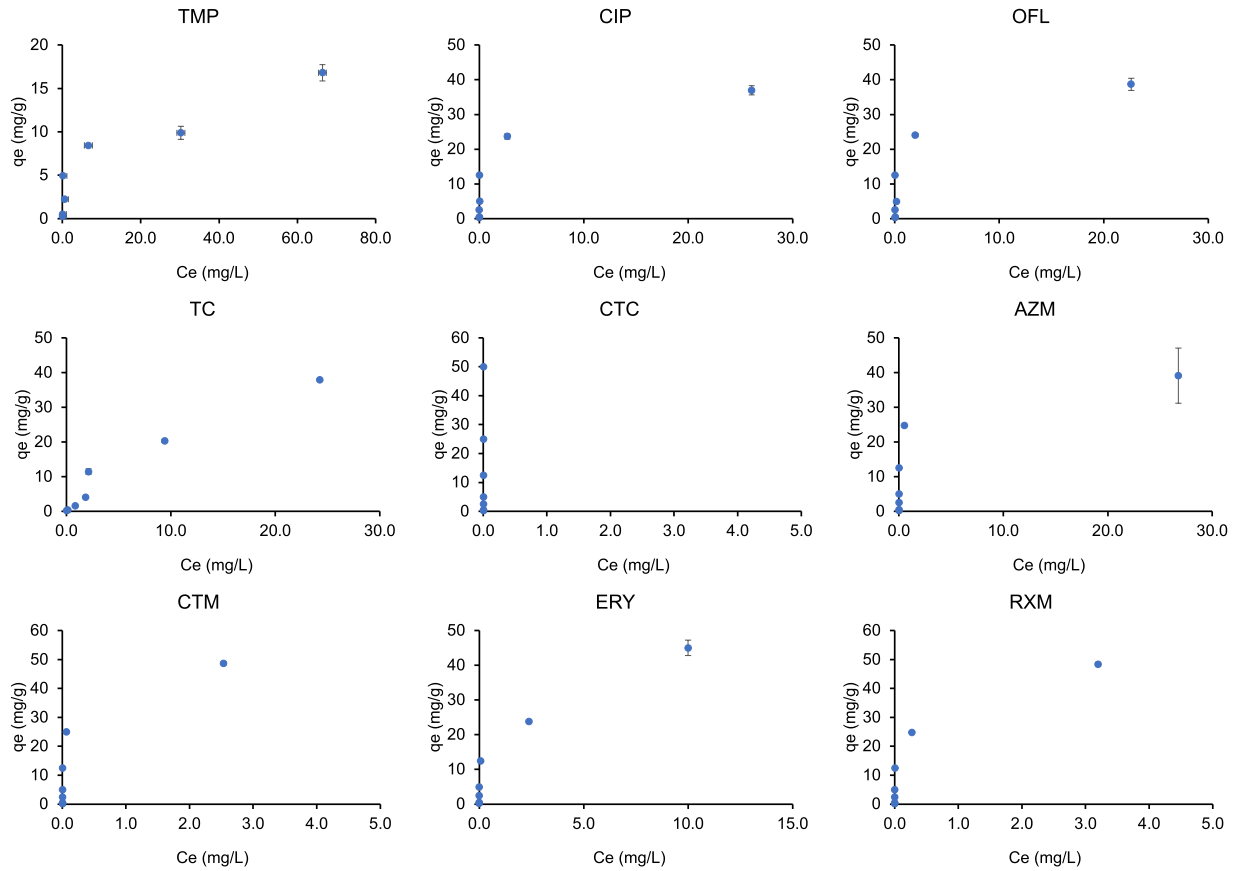| Kinetic parameters	TMP	CIP	OFL	TC	CTC	AZM	CTM	ERY	RXM
Pseudo-first order:									
K_1 (1/min)	13.11 ± 3.43	73.96 ± 7.94	44.88 ± 8.81	5.980 ± 0.005	430.4 ± 0.1	61.09 ± 5.74	47.38 ± 5.22	34.88 ± 4.04	60.97 ± 7.23
q^e_{cal} (mg/g)	0.67 ± 0.02	0.75 ± 2.85	0.53 ± 0.01	0.72 ± 0.01	0.75 ± 0.01	0.75 ± 0.01	0.75 ± 0.01	0.74 ± 0.01	0.74 ± 0.01
q^e_{exp} (mg/g)	0.71	0.75	0.54	0.75	0.75	0.75	0.75	0.75	0.74
R^2	0.868	0.999	0.997	0.959	1.000	0.999	0.999	0.996	0.999
Pseudo-second order:									
K_2 (g/mg·min)	29.68 ± 8.66	4160 ± 947.5	655.4 ± 283.6	565.4 ± 113.1	1E15 ± 7E13	1742 ± 349.0	1048 ± 17.46	222.8 ± 36.10	1505 ± 334.9
q^e_{cal} (mg/g)	0.684 ± 0.017	0.749 ± 2.041	0.533 ± 0.003	0.724 ± 0.013	0.75 ± 0	0.749 ± 0	0.747 ± 0	0.748 ± 0.002	0.744 ± 0
q^e_{exp} (mg/g)	0.71	0.75	0.54	0.75	0.75	0.75	0.75	0.75	0.74
R^2	0.927	0.999	0.998	0.960	0.999	0.999	0.999	0.999	0.999

Fig. 4. Adsorption isotherms of solutions of antibiotics onto MET/ST bionanocomposite.

Table 2
Adsorption isotherm parameters for adsorption of antibiotics onto MET/ST bionanocomposite.

Model parameters	TMP	CIP	OFL	TC	CTC	AZM	CTM	ERY	RXM
Langmuir									
q_{max} (mg/g)	21.5 ± 3.2	100.5 ± 7.7	119.1 ± 9.9	235.0 ± 44.2	28168 ± 10587	117.7 ± 12.3	1194 ± 103	383.1 ± 14.2	1020 ± 62
K_L (L/mg)	0.03 ± 0.01	0.006 ± 0.001	0.005 ± 0.001	0.002 ± 0.001	$2 \cdot 10^{-5} \pm 6 \cdot 10^{-6}$	0.005 ± 0.001	$4 \cdot 10^{-4} \pm 3 \cdot 10^{-5}$	$1 \cdot 10^{-2} \pm 1 \cdot 10^{-4}$	$5 \cdot 10^{-4} \pm 3 \cdot 10^{-5}$
R^2	0.963	0.999	0.999	0.999	0.999	0.998	0.999	0.999	0.999
Freundlich:									
K_F (mg$^{1-1/n}$L$^{1/n}$/g)	1.33 ± 0.40	0.96 ± 0.16	0.89 ± 0.14	0.587 ± 0.002	0.502 ± 0.001	0.92 ± 0.16	0.54 ± 0.01	0.61 ± 0.02	0.54 ± 0.01
n	1.81 ± 0.24	1.25 ± 0.06	1.22 ± 0.05	1.10 ± 0.01	1.00 ± 0.01	1.22 ± 0.06	1.02 ± 0.01	1.07 ± 0.01	1.02 ± 0.01
R^2	0.960	0.995	0.996	0.999	0.999	0.995	0.999	0.999	0.999

maximum for most antibiotics at different temperatures, except for TMP (Figure S4). The lower the temperature, the more effective adsorption of TMP. The negative value of ΔGº indicates that adsorption is spontaneous and feasible in nature and ΔHº was calculated as 9.0 kJ/mol, showing the presence of a physical adsorption process. The positive values of ΔHº and ΔSº confirm that the adsorption nature was endothermic and reflecting the affinity of the MET/ST bionanocomposite for TMP, while the low values of ΔSº was indicative of an increased randomness at the solid-liquid interface. Moreover, ΔG° values between 0 and −20 kJ/mol indicate a physisorption process. Similar results have also been reported elsewhere (Ahmad and Mirza, 2017; 2015).

3.2.3. Influence of environmental conditions: pH, salt and organic content

The pH is one of the factors that influence the adsorption of pollutants on the surfaces of the adsorbent. The change in pH modifies the adsorption through the dissociation of the functional groups present on the surface of the adsorbent. The effect of pH on the adsorptive capacity of MET/ST was evaluated between 2 and 13.

As shown in Figure S5, the adsorbent capacity of MET/ST was close to 100% for most antibiotics, except at very extreme pH. A drastic decrease in the adsorption capacity was observed at values of very acidic pH (2) in the case of the macrolides group and at values of very basic pH (12) for the fluoroquinolones group, probably explained by the low stability of the former and repulsive forces in the latest. In the case of TMP when pH increases between 4 and 9, the adsorption capacity decreases. TMP can be negatively charged at higher pH values, giving rise to electrostatic repulsions with the negatively charged MET/ST bionanocomposite. According to their pK_a values, TMP molecules are positively charged at pH < 3.23, neutral at 3.23 < pH < 6.76 and negatively charged at pH > 6.76. Because macrolides and tetracyclines ionize to form the positive ion, they tend to be adsorbed to the negative charge of MET/ST bionanocomposite surfaces by electrostatic attraction. In the case of fluoroquinolones, they exhibit three dissociation forms, i.e. cationic, zwitterionic and anionic, in water under different pH, however, the last one was only present at very high pH (>9) and is not affected by the removal rate in the range 4–9.

The influence of ionic strength and dissolved organic matter on antibiotic adsorption in MET/ST was evaluated using NaCl (from 0% to 4% v/v) and humic acid solutions (from 0 to 25 mg/L) at constant antibiotic mixture concentration (1500 ng/mL). The low effect of both variables on the adsorption capacity was demonstrated in Figures S6 and S7. The removal efficiency was constant at all concentrations, except for TMP which experimented a significant decrease from 87% to 37% at 0 and 4% v/v of NaCl, respectively. This fact can be explained by a competition effect of Na$^+$ with TMP species for adsorption sites. Similar data was also reported by Maged et al. (2020).

3.3. Mechanism study

The adsorption process consists of complex processes that depend on many factors related to the adsorbate, the adsorbent, and the aqueous medium. According to EDS results (Fig. 5), the percentage of C, N and O in the MET/STV bionanocomposite increased significantly after adsorption (from 0% to 17.88%, from 0% to 1.16% and from 19.58% to 42.91%, respectively) which are the main elements in antibiotic structures and confirm their presence in the adsorbent. Furthermore, the increase in F (from 0% to 2%) could be associated with the presence of fluoroquinolones in the adsorbent (OFL and CIP). Fig. 5 shows the changes in the surface of the adsorbent, it becomes smoother and flaky after antibiotic adsorption. Similar results were also obtained previously (Ahmad and Ansari, 2022).

XRD characterization after adsorption of the antibiotics shows a remarkable decrease in the intensity of peaks existing before adsorption, with the presence of new peaks intensities, 23.7°, 29.48°, 31.53°, 39°, 47.03°, and 48.56° corresponding to a d-spacing of 0.375, 0.303, 0.284, 0.231, 0.193, and 0.188 nm, respectively (Fig. 1, down). This confirms the adsorption of antibiotics on the surface of the material. Furthermore, it is possible to evaluate the mechanism using the FTIR spectrum before and after antibiotic adsorption (Fig. 2, bottom). The adsorption of antibiotics caused a change in the intensity and position of the adsorbent bands. Peaks become more intense in all cases. The adsorption of the antibiotics on the surface of the MET/ST was confirmed by the presence of two intense bands (Fig. 2, down), the first at 1600 cm^{-1} corresponding to stretching deformation combination of H$_2$O ((υ+δ)$_{H_2O}$) and the other at 1370 cm^{-1} of the carbonyl (CO—) group. The rapid adsorption at the initial contact time could be possible due to the antibiotic
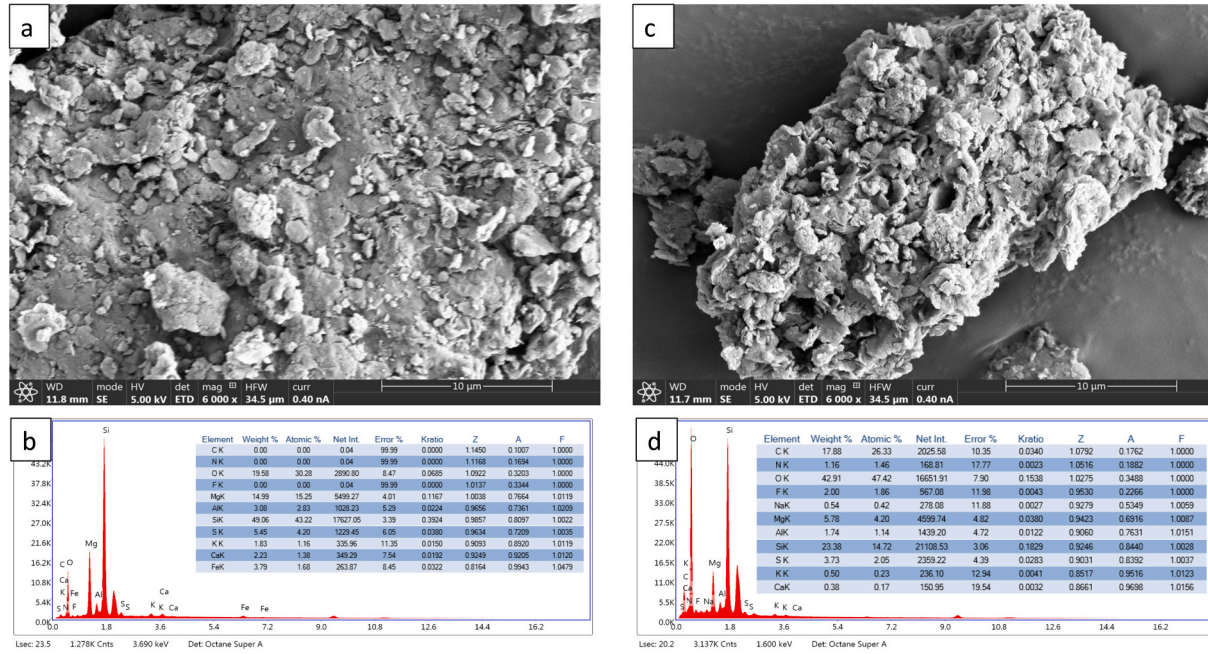
Fig. 5. SEM/EDS characterization of MET/ST before (a/b) and after (c/d) adsorption of antibiotics.
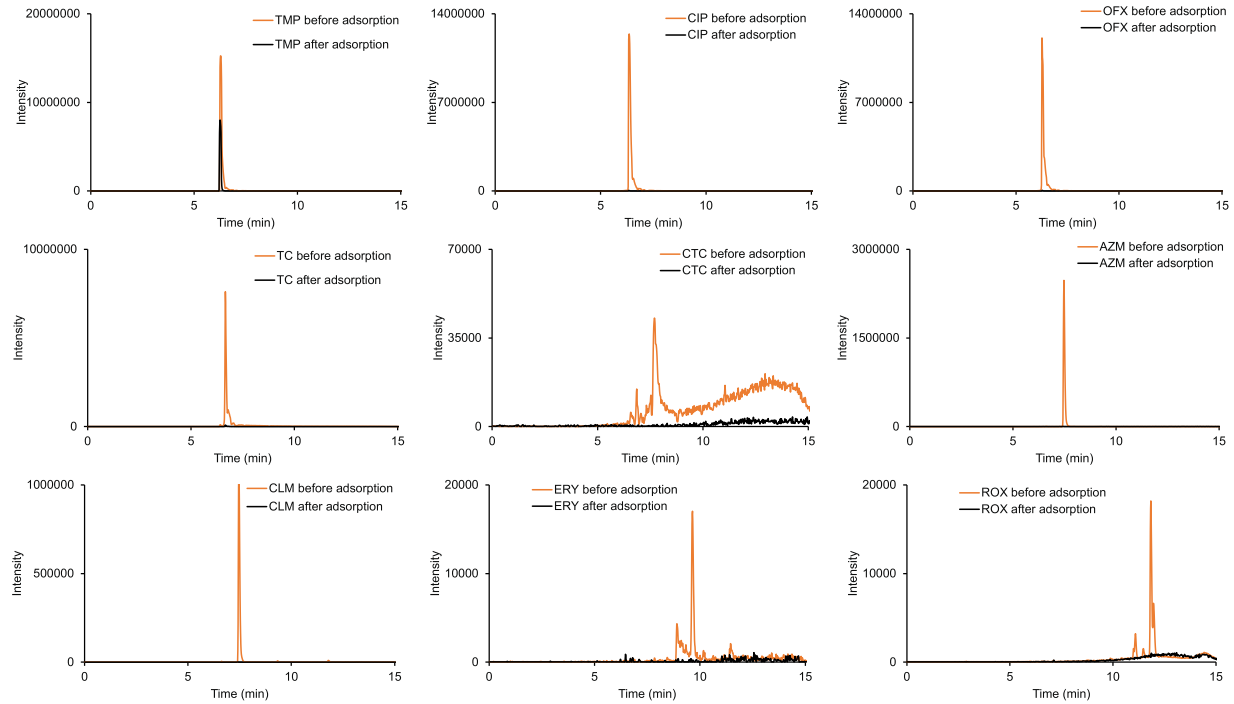
Fig. 6. MRM chromatograms of a spiked effluent wastewater sample (1.5 mg/L) before and after the adsorption onto MET/ST bionanocomposite.

binding to the MET/ST bionanocomposite by electrostatic forces between the positively charged antibiotics and the negatively charged surface of the MET/ST, as well as being housed in the interlaminar space of the clay (Antón-Herrero et al., 2018). This fact is in concordance with the measurement of the zeta potential (Table S4). The MET/ST bionanocomposite presents a negative zeta potential before adsorption (-11.1 mV, pH = 5), while it turned into positive values after adsorption of antibiotics (+2.16 mV).

Hydrogen bonding could be present in the adsorption mechanism. Carboxyl and amine groups of MET immobilised in the ST matrix can provide active sites for dipole interactions. In the 3700–2500 cm^{-1} region, O–H and N–H frequencies are present, and hydrogen bonding influences the peak shapes (Van Eerdenbrugh et al., 2011). The bands in this region reduced their intensity after adsorption (Fig. 2). These changes could indicate the presence of intermolecular hydrogen bonding, which can be explained by the interactions between the O–H and N-H groups of MET and the O–H and N–H groups of antibiotics. Furthermore, n-p interactions can be created between the Si-O-Si bonds in the MET/STV-derived bionanocomposite structure and the aromatic structure of antibiotics.

Furthermore, another possible mechanism could be pore filling, which is based on the ability of the antibiotics to occupy and fill in the pores present on the surface of the MET/STV derived bionanocomposite. The porous structure and high specific surface area of MET/ST can adsorb large amounts of antibiotics. MET/ST contains many mesopores with a pore size of 7.06 nm and a pore volume of 0.16 cm^3/g, which can provide sufficient area for pollutant adsorption. In fact, after the adsorption process, both the specific surface area and the pore volume were considerably reduced (from 170 to 14 m^2/g and from 0.16 to 0.05 cm^3/g) (Table S4).

On the basis of all of the above, a physisorption mechanism for MET/STV-antibiotic interactions including pore filling, electrostatic, hydrophobic, or hydrogen bonding types are proposed.

3.4. Desorption and reuse

The reuse of the adsorbent is crucial to its economic feasibility and application in the field of water purification. Figure S8 shows the antibiotic removal efficiency by MET/ST sample after four consecutive cycles. The adsorbed MET/ST sample was treated with 5 mL of methanol + 5 mL of HCl (0.1 M) and rinsed with deionized water after each cycle. Acidic eluents provide high concentration of

Table 3

Adsorption capacity of different contaminants by amino acids-clays materials and other bipolymers-clays materials.

Adsorbent material	Pollutant		Adsorption capacity (mg/g)	References
Amino acids-clays materials				
MET-Montmorillonite	AZM		298.78	Imanipoor et al., 2021a
MET-Montmorillonite	Amoxicilline		647.7	Imanipoor et al., 2021b
L-Histidine-Montmorillonite	Acetaminophenol		8.23	Chu et al., 2019a
L-Arginine-Montmorillonite			8.45	
MET-Montmorillonite			7.18	
L-Cysteine-Chitosan-Bentonite	Cristal violet		240	Ahmad and Ezaj, 2023
MET-Kaollinite-Cellulose	Amido Black 10B dye		172.14	Ahmad and Ansari, 2022
L-Histidine-Bentonite	Cu		4.995	Bakatula et al., 2014
		Ni	4.986	
		Zn	4.998	
		Co	4.998	
		Fe	4.998	
		Hg	4.993	
		U	4.994	
L-Arginine-Montmorillonite	Pb		124.69	Chu et al., 2019b
		Cu	29.15	
MET-Montmorillonite	Pb		117.79	Chu et al., 2020
L-Lysine-Montmorillonite	Pb		335	Boahen et al., 2023
		Cu	108.4	
		Ni	77.48	
Polysulfone-L-Arginine-Montmorillonite	As		16.5	Shokri et al., 2017
L-Cysteine-Montmorillonite	Co		830	El Adraa et al., 2017
		Ni	864	
		Cu	917	
		Zn	891	
		Cd	853	
		Hg	868	
		Pb	876	
L-Histidine-Montmorillonite	As		87.7	Batool et al., 2022
L-Lysine-Montmorillonite	Pb		89.71	Zhu et al., 2019
L-Cysteine-Beidellite	Cu		155	Brigatti et al., 2004
Biopolymer-clays materials				
Zr/Chitosan/Perlite clay	TC		104.17	Turan et al., 2022
Alginate-Bentonite	Doripenem		49.89	Yuliana et al., 2022
Chitosan-Bentonite	Doripenem		96	Yeo et al., 2023
	Amoxicillin		86.1	
	Ampicillin		83.3	
Chitosan–Alginate–Bentonite	TC		178.65	Nunes-Filho et al., 2023

hydronium ions that reduce the attraction of the adsorbate toward the adsorbent active groups and allow desorption utilizing ion exchange mechanisms, while methanol, because of its small and polar molecules, can access the adsorbent interlayer space, interact with the adsorbate functional groups, and then desorb the adsorbate molecules. From the cycling results, seven out of nine antibiotics could be desorbed > 97% after the four cycles. The removal efficiency of TMP (87%) and ERY (99%) decreased to 41% and 62%, respectively, after four cycles. The excellent regeneration capability is the main source of value for an adsorbent. This study suggests the potential to reduce the costs associated with the procedure.

3.5. Adsorption in environmental real matrices

Finally, simulated systems are mandatory to evaluate their real application. To achieve environmental realism, the adsorption test was performed using fortified environmental real waters (influent and effluent wastewater, surface water and tap water). The samples were filtered through a 1.2 μm glass-microfiber membrane filter. Quantification was carried out using matrix-matched calibration curves.

The proposed adsorbent presented an adsorption rate >91% for most antibiotics, which is extremely high value considering the complexity of the matrices (Figure S9). The adsorption of TMP was the only one affected by the matrix, decreasing its removal efficiency from 87% in distilled water to 69% in surface water and 55% in effluent wastewater. The influent wastewater samples also led to a slight decrease of 10% in the adsorption capacity of MET/ST for TC (Figure S9). For instance, after spiked, in effluent wastewater, the concentrations of antibiotics were between 1.33 mg/L (TC) to 1.92 (TMP) mg/L. After a contact time of 60 min with 20 mg of material, the total adsorbed amount of antibiotics decreased to 0.864 mg/L and 0.07 mg/L for TMP and TC, respectively, which means a total removal between 55% for TMP and >94% for the rest of antibiotics (see a MRM chromatogram of an effluent wastewater sample in Fig. 6).

A comparative study on the adsorption capacity of clays and organomodified clays is presented in Table 3. Ancient studies have been devoted to possible applications of ST in the field water treatment for the removal of heavy metals (Benhammou et al., 2005), dye (Elass et al., 2011) and more recent phenol compounds (Hnana et al., 2019; Hamdaoui et al., 2018). There are also some novel studies linking the amino acid MET with clay minerals for the removal of heavy metals or AZM as model compounds. MET-modified bentonite/alginate nanocomposite was used as an adsorbent for the elimination of Pb(II) and Cd(II) with an effective removal of up to about 98% and 82%, respectively (Ahmad and Mirza, 2015). Imanipoor et al. (2021a) examined the adsorptive removal of AZM on MET-modified montmorillonite. The results revealed a removal efficiency of 98% using an adsorbent dosage of 0.5 g/L and a AZM concentration of 50 mg/L. To our knowledge, this is the first time that a bionanocomposite has been applied as adsorbent of a wide group of antibiotics. Another innovative element of this study is its application to real environmental samples, most studies on drug adsorption have been carried out under batch and ideal conditions with distilled water.

4. Conclusions

In the present work, a novel bionanocomposite (MET/ST) was synthesized and evaluated as an effective adsorbent for the removal of a wide group of antibiotics including TMP, CIP, OFL, TC, CTC, AZM, CTM, ERY, and RXM. Based on the results obtained, MET/ST is a good adsorbent for the removal of antibiotics from environmental water samples. Its unique properties, such as low toxicity, high stability, and abundant occurrence in natural sources, make this material a promising alternative for the treatment of environmental pollutants. The adsorption kinetic was fitted to the pseudo-second order model. The equilibrium was achieved in less than 1 min for most of antibiotics (except TMP) and a removal efficiency of close to 100% was observed in a wide range of pH scale (4−9). The maximum sorption capacity was determined with the Langmuir and Freundlich isotherms (from 21.48 mg/g for TMP to > 110 mg/g for the rest of antibiotics). MET/ST can be used as a reusable adsorbent (up to four cycles) for convenient, easy, and efficient removal of antibiotics from water. The ability of ST to adsorb antibiotics was strengthened by their characteristics; their combination with MET helped pave the way to green bionanocomposite production. Major efforts are still required to scale up to the pilot plant level performing dynamic adsorption studies using columns. Furthermore, in-depth analyses on the interaction of bionanomaterials with other environmental matrices need to be considered.

CRediT authorship contribution statement

Esteban Alonso: Supervision, Project administration, Funding acquisition, Conceptualization. **Irene Aparicio:** Visualization, Project administration, Funding acquisition. **Mohamed Choukairi:** Visualization. **Juan Luis Santos:** Writing – review & editing, Visualization, Methodology, Funding acquisition. **Carmen Mejías:** Resources, Methodology, Investigation. **Loubna Bounab:** Visualization. **Moaad Gharous:** Writing – original draft, Resources, Investigation, Conceptualization. **Julia Martín:** Writing – review & editing, Writing – original draft, Resources, Methodology, Investigation, Conceptualization.

Declaration of Competing Interest

The authors declare that they have no known competing financial interests or personal relationships that could have appeared to influence the work reported in this paper.

Data availability

Data will be made available on request.

Acknowledgements

Appendix A. Supporting information

Supplementary data associated with this article can be found in the online version at doi:10.1016/j.eti.2024.103591.

References

Ahmad, R., Ansari, K., 2022. Novel in-situ fabrication of L-methionine functionalized bionanocomposite for adsorption of Amido Black 10B dye. Process Biochem 119, 48–57. https://doi.org/10.1016/j.procbio.2022.05.015.

Ahmad, R., Mirza, A., 2015. Sequestration of heavy metal ions by methionine modified bentonite/alginate (Methbent/Alg): a bionanocomposite. Ground Sustain Dev. 1 (1-2), 50–58. https://doi.org/10.1016/j.gsd.2015.11.003.

Ahmad, R., Mirza, A., 2017. Green synthesis of Xanthan gum/Methionine-bentonite nanocomposite for sequestering toxic anionic dye. Surf. Interfaces 8, 65–72. https://doi.org/10.1016/j.surfin.2017.05.001.

Ahmad, R., Ejaz, M.O., 2023. Efficient adsorption of crystal violet (CV) dye onto benign chitosan-modified l-cysteine/bentonite (CS-Cys/Bent) bionanocomposite: synthesis, characterization and experimental studies. Dyes Pigments 216, 111305. https://doi.org/10.1016/j.dyepig.2023.111305.

Ahrouch, M., Gatica, J.M., Draoui, K., Bellido, D., Vidal, H., 2019. Lead removal from aqueous solution by means of integral natural clays honeycomb monoliths. J. Hazard Mat. 365, 519–530. https://doi.org/10.1016/j.jhazmat.2018.11.037.

Ajbary, M., Santos, A., Morales-Flórez, V., Esquivias, L., 2013. Removal of basic yellow cationic dye by an aqueous dispersion of Moroccan stevensite. Appl. Clay Sci. 80–81, 46–51. https://doi.org/10.1016/j.clay.2013.05.011.

Allaoui, S., Bennani, M.N., Ziyat, H., Qabaqous, O., Tijani, N., Ittobane, N., 2020. Kinetic study of the adsorption of polyphenols from olive mill wastewater onto natural clay: ghassoul. J. Chem., 7293189 https://doi.org/10.1155/2020/7293189.

Anjali, R., Shanthakumar, S., 2019. Insights on the current status of occurrence and removal of antibiotics in wastewater by advanced oxidation processes. J. Environ. Manag 246, 51–62. https://doi.org/10.1016/j.jenvman.2019.05.090.

Antón-Herrero, R., García-Delgado, C., Alonso-Izquierdo, M., García-Rodríguez, G., Cuevas, J., Eymar, E., 2018. Comparative adsorption of tetracyclines on biochars and stevensite: looking for the most effective adsorbent. Appl. Clay Sci. 160, 162–172. https://doi.org/10.1016/j.clay.2017.12.023.

Attallah, O.A., Al-Ghobashy, M.A., Nebsen, M., Salem, M.Y., 2016. Adsorptive removal of fluoroquinolones from water by pectin-functionalized magnetic nanoparticles: process optimization using a spectrofluorimetric assay. ACS Sustain. Chem. Eng. 5, 133–145. https://doi.org/10.1021/acssuschemeng.6b01003.

Azaryouh, L., Abara, H., Kassab, Z., Ablouh, E., Aboulkas, A., El Achaby, M., Draoui, K., 2023. Hybrid carbonaceous adsorbents based on clay and cellulose for cadmium recovery from aqueous solution. RSC Adv. 13, 6954–6965. https://doi.org/10.1039/d2ra08287j.

Bakatula, E.N., Cukrowska, E.M., Weiersbye, I.M., Mihaly-Cozmuta, L., Tutu, H., 2014. Removal of toxic elements from aqueous solution using bentonite modified with L-histidine. Water Sci. Technol. 70 (12), 2022–2030. https://doi.org/10.2166/wst.2014.450.

Batool, A., Shah, K.H., Hussain, S., Hussain, Z., Naqvi, S.A.R., Sherazi, T.A., 2022. L-Histidine immobilized montmorillonite for As(III) adsorption and statistical verification of data by PDF, AICcorrected and AADR models. Appl. Water Sci. 12, 258. https://doi.org/10.1007/s13201-022-01777-2.

Ben Seddik, N., Raissouni, I., Draoui, K., Aghzzaf, A.A., Chraka, A., Aznag, B., Chaouket, F., Bouchta, D., 2019. Calcite, the main corrosion inhibitor contained in the raw clay (Rhassoul) of brass in 3% NaCl medium. Mediterr. J. Chem. 9 (3) https://doi.org/10.13171/mjc93191016530nbs.

Ben Amor, A., Arenas, M., Martín, J., Ouakouak, A., Santos, J.L., Aparicio, I., Alonso, E., Hamdi, N., 2023. Alginate/geopolymer hybrid beads as an innovative adsorbent applied to the removal of 5-fluorouracil from contaminated environmental water. Chemosphere 335, 139092. https://doi.org/10.1016/j.chemosphere.2023.139092.

Benhammou, A., Yaacoubi, A., Nibou, L., Tanouti, B., 2005. Adsorption of metal ions onto Moroccan stevensite: kinetic and isotherm studies. J. Colloid Interface Sci. 282 (2), 320–326. https://doi.org/10.1016/j.jcis.2004.08.168.

Bentahar, Y., Draoui, K., Hurel, C., Khairoun, S., Ajouyed, O., Marmier, N., 2019. Physico-chemical characterization and valorization of swelling and nonswelling Moroccan clays in basic dye removal from aqueous solutions. J. Afr. Earth Sci. 154, 80–88. https://doi.org/10.1016/j.jafrearsci.2019.03.017.

Boahen, C., Wiafe, S., Ozusu, F., Bian, L., 2023. Adsorption of heavy metals from mine wastewater using amino-acid modified Montmorillonite. Sustain Environ. 9 (1), 2152590 https://doi.org/10.1080/27658511.2022.2152590.

Brandão-Lima, L.C., Silva, F.C., Costa, P.V.C.G., Alves-Júnior, E.A., Viseras, C., Osajima, J.A., Bezerra, L.R., de Moura, J.F.P., Silva, A.G.A., Fonseca, M.G., Silva-Filho, E.C., 2022. Clay mineral minerals as a strategy for biomolecule incorporation: amino acids approach. Materials 15 (1), 64. https://doi.org/10.3390/ma15010064.

Brião, G.V., da Silva, M.G.C., Vieira, M.G.A., Chu, K.H., 2022. Correlation of type II adsorption isotherms of water contaminants using modified BET equations. Colloid Interface Sci. Commun. 46, 100557 https://doi.org/10.1016/j.colcom.2021.100557.

Brigatti, M.F., Malferrari, D., Medici, L., Poppi, L., 2004. Effect of amino acids on the retention of copper by beidellite. Environ. Eng. Sci. 20 (6) https://doi.org/10.1089/109287503770736113.

Cao, H.L., Cai, F.Y., Yu, K., Zhang, Y.Q., Luï, J., Cao, R., 2019. Photocatalytic degradation of tetracycline antibiotics over CdS/nitrogen-doped–carbon composites derived from in situ carbonization of metal–organic frameworks. ACS Sustain. Chem. Eng. 7, 10847–10854. https://doi.org/10.1021/acssuschemeng.9b01685.

Chaturvedi, P., Giri, B.S., Shukla, P., Gupta, P., 2021. Recent advancement in remediation of synthetic organic antibiotics from environmental matrices: challenges and perspective. Bioresour. Technol. 319, 124161 https://doi.org/10.1016/j.biortech.2020.124161.

Chu, Y., Khan, M.A., Xia, M., Lei, W., Wang, F., Zhu, S., 2019a. Synthesis and mechanism of adsorption capacity of modified montmorillonite with amino acids for 4-acetaminophenol removal from wastewaters. J. Chem. Eng. Data 64 (12), 5900–5909. https://doi.org/10.1021/acs.jced.9b00795.

Chu, Y., Khan, M.A., Wang, F., Xia, M., Lei, W., Zhu, S., 2019b. Kinetics and equilibrium isotherms of adsorption of Pb(II) and Cu(II) onto raw and arginine-modified montmorillonite. Adv. Powder Technol. 30 (5), 1067–1078. https://doi.org/10.1016/j.apt.2019.03.002.

Chu, Y., Zhu, S., Xia, M., Wang, F., Lei, W., 2020. Methionine-montmorillonite composite – a novel material for efficient adsorption of lead ions. Adv. Powder Technol. 31, 708–717. https://doi.org/10.1016/j.apt.2019.11.026.

de Santiago-Buey, C., Suárez-Barrios, M., García-Romero, E., Doval-Montoya, M., 2000. Mg-Rich Smectite "precursor" Phase in the Tagus Basin, Spain. Clays Clay Min. 48, 366–373. https://doi.org/10.1346/CCMN.2000.0480307.

Delgado, N., Orozco, J., Zambrano, S., Casas-Zapata, J.C., Marino, D., 2023. Veterinary pharmaceutical as emerging contaminants in wastewater and surface water: an overview. J. Hazard Mat. 460, 132431 https://doi.org/10.1016/j.jhazmat.2023.132431.

Dutta, J., Mala, A.A., 2020. Removal of antibiotic from the water environment by the adsorption technologies: a review. Water Sci. Technol. 82, 401–426. https://doi.org/10.2166/wst.2020.335.

El Adraa, K., Georgelin, T., Lambert, J.F., Jaber, F., Tielens, F., Jaber, M., 2017. Cysteine-montmorillonite composites for heavy metal cation complexation: a combined experimental and theoretical study. Chem. Eng. J. 314, 406–417. https://doi.org/10.1016/j.cej.2016.11.160.

El Mahbouby, A., Ezaier, Y., Zyade, S., Mechnou, I., 2023. Elaboration and characterization of organo-ghassoul (moroccan clay) as an adsorbent using cationic surfactant for anionic dye adsorption. Phys. Chem. Res 11 (4), 913–928. https://doi.org/10.22036/pcr.2022.365510.2221.

Elass, K., Laachach, A., Alaoui, A., Azzi, M., 2011. Removal of methyl violet from aqueous solution using a stevensite-rich clay from Morocco. Appl. Clay Sci. 54 (1), 90–96. https://doi.org/10.1016/j.clay.2011.07.019.

European Commission, 2018. EUR-Lex – commission implementing decision (EU) 2018/ 840 of 5 June 2018 establishing a watch list of substances for Union-wide monitoring in the field of water policy pursuant to Directive 2008/105/EC of the European Parliament and of the Council and repealing Commission Implementing Decision (EU) 2015/495. Off J Eur Union L141, 9–12.

European Commission, 2020. Regulation (EU) 2020/741 of the European Parliament and of the Council of 25 May 2020 on Minimum Requirements for Water Reuse.

European Commission, 2022. Commission Implementing Decision (EU) 2022/1307 of 22 July 2022 establishing a watch list of substances for Union-wide monitoring in the field of water policy pursuant to Directive 2008/105/EC of the European Parliament and of the Council.

Faghihian, H., Nejati-Yazdinejad, M., 2009. Sorption performance of cysteine- modified bentonite in heavy metals uptake. J. Serb. Chem. Soc. 74 (7), 833–843. https://doi.org/10.2298/JSC0907833F.

Fernández, R., Ruiz, A.I., García-Delgado, C., González-Santamaría, D.E., Antón-Herrero, R., Yunta, F., Poyo, C., Hernández, A., Eymar, E., Cuevas, J., 2018. Stevensite-based geofilter for the retention of tetracycline from wáter. Sci. Total Environ. 645, 146–155. https://doi.org/10.1016/j.scitotenv.2018.07.120.

Hacıosmanoglu, G.G., Arenas, M., Mejías, C., Martín, J., Santos, J.L., Aparicio, I., Alonso, E., 2023. Adsorption of fluoroquinolone antibiotics from wáter and wastewapr by colemanite. Int J. Environ. Res Public Health 20 (3), 2646. https://doi.org/10.3390/ijerph20032646.

Hamdaoui, M., Hadri, M., Bencheqroz, Z., Draoui, H., Nawdali, M., Zaitan, M., Barhoun, A., 2018. Improvement of phenol removal from aqueous medium by adsorption on organically functionalized Moroccan stevensite. J. Mat. Environ. Sci. 9 (4), 1119–1128. https://doi.org/10.26872/jmes.2018.9.4.123.

Hnana, K., Barhoun, A., Draoui, K., 2019. Improvement of glyphosate adsorption using new composites based on ghassoul and chitosan: kinetics and equilibrium study. Mediterr. J. Chem. 9 (4) https://doi.org/10.13171/mjc9419111121087kd.

Imanipoor, J., Mohammadi, M., Dinari, M., 2021a. Evaluating the performance of L-methionine modified montmorillonite K10 and 3-aminopropyltriethoxysilane functionalized magnesium phyllosilicate organoclays for adsorptive removal of azithromycin from water. Sep Purif. Technol. 275, 119256 https://doi.org/10.1016/j.seppur.2021.119256.

Imanipoor, J., Ghafelebashi, A., Mohammadi, M., Dinari, M., Ehsani, M.R., 2021b. Fast and effective adsorption of amoxicillin from aqueous solutions by L-methionine modified montmorillonite K10. Colloids Surf. A Physicochem Eng. Asp. 611, 125792 https://doi.org/10.1016/j.colsurfa.2020.125792.

Khan, S.A., Khan, T.A., 2021. Clay-hydrogel nanocomposites for adsorptive amputation of environmental contaminants from aqueous phase: a review. J. Environ. Chem. Eng. 9 (4), 105575 https://doi.org/10.1016/j.jece.2021.105575.

Kianfar, A.H., Mahmood, W.A.K., Dinari, M., Azarian, M.H., Khafri, F.Z., 2014. Novel nanohybrids of cobalt (III) Schiff base complexes and clay: synthesis and structural determinations. SAA Spectrochim. Acta Part A Molec Biomolec Spectros. 127, 422–428. https://doi.org/10.1016/j.saa.2014.02.089.

Kolya, H., Kang, C.W., 2023. Next-generation water treatment: exploring the potential of biopolymer-based nanocomposites in adsorption and membrane filtration. Polymers 15, 3421. https://doi.org/10.3390/polym15163421.

Kuroki, V., Bosco, G.E., Fadini, P.S., Mozeto, A.A., Cestari, A.R., Carvalho, W.A., 2014. Use of a La(III)-modified bentonite for effective phosphate removal from aqueous media. J. Hazard Mat. 274, 124–131. https://doi.org/10.1016/j.jhazmat.2014.03.023.

Maged, A., Iqbal, J., Kharbish, S., Ismael, I.S., Bhatnagar, A., 2020. Tuning tetracycline removal from aqueous solution onto activated 2:1 layered clay mineral: characterization, sorption and mechanistic studies. J. Hazard Mater. 384 https://doi.org/10.1016/j.jhazmat.2019.121320.

Mallakpour, S., Dinari, M., 2011. Biomodification of cloisite Na1 with L-methionine amino acid and preparation of poly(vinyl alcohol)/organoclay nanocomposite films. J. Appl. Polym. Sci. 124 (5), 4322–4330. https://doi.org/10.1002/app.35540.

Martín, J., Orta, M.M., Medina-Carrasco, S., Santos, J.L., Aparicio, I., Alonso E., Biodegradable Polymers and Their Bionanocomposites Based on Layered Silicates: Environmental Applications. Pag. 1-30. En: Biodegradable and Environmental Applications of Bionanocomposites. Advanced Structured Materials. Switzerland. Springer, Cham. 2023. ISBN 978-3-031-13342-8.

Mejías, C., Martín, J., Santos, J.L., Aparicio, I., Sánchez, M.I., Alonso, E., 2022. Development and validation of a highly effective analytical method for the evaluation of the exposure of migratory birds to antibiotics and their metabolites by faeces analysis. Anal. Bioanal. Chem. 414, 3373–3386. https://doi.org/10.1007/s00216-022-03953-4.

Mejías, C., Martín, J., Santos, J.L., Aparicio, I., Alonso, E., 2021. Occurrence of pharmaceuticals and their metabolites in sewage sludge and soil: a review on their distribution and environmental risk assessment. Trends Environ. Anal. Chem. 30, e00125 https://doi.org/10.1016/j.teac.2021.e00125.

Moussout, H., Ahlafi, H., Aazza, M., Chfaira, R., Mounir, C., 2020. Interfacial electrochemical properties of natural Moroccan Ghassoul (stevensite) clay in aqueous suspension. Heliyon 6 (3), e03634. https://doi.org/10.1016/j.heliyon.2020.e03634.

Naboulsi, A., El Himri, M., Gharibi, E.K., El Haddad, M., 2022. Study of adsorption mechanism of Malachite Green (MG) and Basic Yellow 28 (BY28) onto smectite rich natural clays (Ghassoul) using DFT/B3LYP and DOE/FFD. Surf. Interfaces 33, 102227. https://doi.org/10.1016/j.surfin.2022.102227.

Nunes-Filho, F.G., Silva-Filho, E.C., Osajima, J.A., de Melo-Alves, A.P., Fonseca, M.G., 2023. Adsorption of tetracycline using chitosan–alginate–bentonite composites. Appl. Clay Sci. 239, 106952 https://doi.org/10.1016/j.clay.2023.106952.

Oberoi, A.S., Jia, Y., Zhang, H., Khanal, S.K., Lu, H., 2019. Insights into the fate and removal of antibiotics in engineered biological treatment systems: a critical review. Environ. Sci. Technol. 53, 7234–7264. https://doi.org/10.1021/acs.est.9b01131.

Orta, M.M., Martín, J., Medina-Carrasco, S., Santos, J.L., Aparicio, I., Alonso, E., 2020. Biopolymer-clay nanocomposites as novel and ecofriendly adsorbents for environmental remediation. Appl. Clay Sci. 198, 105838 https://doi.org/10.1016/j.clay.2020.105838.

Pereira, A.G.B., Rodrigues, F.H.A., Paulino, A.T., Martins, A.F., Fajardo, A.R., 2021. Recent advances on composite hydrogels designed for the remediation of dye-contaminated water and wastewater: a review. J. Clean. Prod. 284, 124703 https://doi.org/10.1016/j.jclepro.2020.124703.

Shokri, E., Yegani, R., Akbarzadeh, A., 2017. Novel adsorptive mixed matrix membranes by embedding modified montmorillonite with arginine amino acid into polysulfones for As(V) removal. Appl. Clay Sci. 144, 141–149. https://doi.org/10.1016/j.clay.2017.05.011.

Tran, N.H., Chen, H., Reinhard, M., Mao, F., Gin, K.Y.H., 2016. Occurrence and removal of multiple classes of antibiotics and antimicrobial agents in biological wastewater treatment processes. Water Res. 104, 461–472. https://doi.org/10.1016/j.watres.2016.08.040.

Turan, B., Sarigol, G., Demircivi, P., 2022. Adsorption of tetracycline antibiotics using metal and clay embedded cross-linked chitosan. Mat. Chem. Phys. 279, 125781 https://doi.org/10.1016/j.matchemphys.2022.125781.

Yeo, J.Y.J., Khaerudini, D.S., Soetaredjo, F.E., Waworuntu, G.L., Ismadji, S., Sunarso, J., Liu, S., 2023. Isotherm data for adsorption of amoxicillin, ampicillin, and doripenem onto bentonite. Data Brief. 48, 109159 https://doi.org/10.1016/j.dib.2023.109159.

Yuliana, M., Ismadji, S., Lie, J., Santoso, S.P., Soetaredjo, F.E., Waworuntu, G., Putro, J.N., Wijaya, C.J., 2022. Low-cost structured alginate-immobilized bentonite beads designed for an effective removal of persistent antibiotics from aqueous solution. Environ. Res 207, 112162. https://doi.org/10.1016/j.envres.2021.112162.

Zhao, S., Ba, C., Yao, Y., Zheng, W., Economy, J., Wang, P., 2018. Removal of antibiotics using polyethylenimine cross-linked nanofiltration membranes: relating membrane performance to surface charge characteristics. Chem. Eng. J. 335, 101–109. https://doi.org/10.1016/j.cej.2017.10.140.

Zhu, S., Xia, M., Chu, Y., Khan, M.A., Lei, W., Wang, F., Muhmood, T., 2019. Adsorption and desorption of Pb(II) on l-lysine modified montmorillonite and the simulation of interlayer structure (Along Wang). Appl. Clay Sci. 169, 40–47. https://doi.org/10.1016/j.clay.2018.12.017.

Ziyat, H., Bennani, M.N., Hajjaj, H., Qabaqous, O., Arhzaf, S., Mekdad, S., Allaoui, S., 2020. Adsorption of thymol onto natural clays of morocco: kinetic and isotherm studies. J. Chem. 4925809. https://doi.org/10.1155/2020/4926809.